

Fabrication of Ag@Cr Core-Shell Nano Composites for NO₂ Gas Sensing Application

Zahraa A. Muqbil^{1*} and Ashwaq T. Dahham¹

¹*Department of Physics, College of Science, University of Baghdad, Baghdad, Iraq*

*Corresponding author: zahraa.Ali1604@sc.uobaghdad.edu.iq

Abstract

In this work, Ag and Ag@Cr nanoparticles were fabricated utilizing the plasma jet and chemical spray deposition approach to produce thin films of Ag and Ag@Cr. The optimal gas-detecting properties can be achieved by varying the ratios of Ag@Cr (4:6, 2:8, 3:7) ml and 10 ml Ag. XRD, transmission electron microscopy (TEM), and UV-Vis spectroscopy were used to characterize the Ag and Ag@Cr thin films. Additionally, an absorption peak appears at 422 nm for Ag, and the absorption peaks for Ag@Cr are at 408, 413, and 410 nm, with a polycrystalline character as seen from the XRD pattern. The gas NO₂ was used to check how sensitive, responsive, and quickly recoverable the Ag and Ag@Cr nanocomposite thin films are. According to the findings, at 150 °C, the optimal Ag@Cr ratio was 3:7 with 26% sensitivity. At 150 °C, pure silver's sensitivity was 32%, and it was concluded that chromium has low sensitivity. The results of the Hall effect test indicated that the material is p-type at all ratios.

Article Info.

Keywords:

NO₂, Gas Sensor, Nanocomposites, Ag@Cr, Core-shell.

Article history:

Received: Jul. 10, 2024

Revised: Nov. 09, 2024

Accepted: Nov. 11, 2024

Published: Jun 01, 2025

1. Introduction

Nitrogen dioxide (NO₂), a combustible gas with a strong odor, is one of the poisonous gases that can harm both humans and the environment [1-4]. With a straight band gap of 1.2 eV, silver dioxide (Ag₂O) is a p-type semiconductor highly recommended for use in gas sensors due to its stability, non-toxicity, affordability, and sensitivity to gases [5-9]. Chromium (Cr) (VI) is recognized as a substance that causes cancer, is highly poisonous, and is not biodegradable. In soil, surface water, and groundwater, Cr is discovered to be a pollutant. People who inhale Cr may get dermatitis and lung and nasopharyngeal carcinoma, among other illnesses [10]. Among the many types of multicomponent heterostructure nanosystems, metal-semiconductor core-shell nanoparticle systems are significant. Localized Surface Plasmon Resonance (LSPR) creates a combination property from distinct components; even greater and new characteristics will develop because of the nanoscale interactions between the various core and shell components [11-13].

A gas sensor is a device that detects gases present in an area, especially those that could be dangerous to people or animals. In recent years, the development of gas sensor technology has drawn a lot of attention to monitoring environmental contamination. It is commonly known that the characteristics of the sensing materials utilized significantly impact on the performance attributes of chemical gas sensors, including sensitivity, selectivity, temporal response, stability, durability, repeatability, and reversibility [14]. A change in the electrical property of the detecting material upon exposure to the gas is the fundamental idea underpinning gas detection [15]. Thin films with various silver and chromium percentages used as the detecting elements were examined in this investigation. The reaction time and recovery time of the manufactured Ag@Cr gas sensors were examined at a varied temperature in addition to sensitivity for gas sensor NO₂.



2. Experimental

In this study, chromium nitrate (99% purity) of (400.15 g/mol wt.) and silver nitrate AgNO_3 (169.872 g/mole) partial weight Ag, 100 ml pure water, 2 mM chromium nitrate, and 1 mM silver nitrate were used. The required weight (0.0169 Ag, 0.0809 Cr) was calculated using the following Eq. (1)

$$\text{Concentration (mole)} = (\text{mass (g)}) / (\text{Molecular weight (g / mol)} \times \text{volume (liter)}) \quad (1)$$

Plasma, which was used to synthesize the silver nanoparticles, was formed by applying a high voltage of about 17 kV between the filament and the aqueous solution of AgNO_3 under a pressure of 3 L/min; The exposure time of 6 minutes was chosen for the (10 ml) volume. After a few minutes of starting the discharge, the solution starts to turn yellow, which is evidence of the formation of silver nanoparticles. Using chromium nitrate as the Cr source, Cr solution (8, 7, and 6 mL) was added to the silver nanoparticles solution (2, 3 and 4 mL), and the solution was stirred for 5 minutes. Then the prepared glass beaker was placed on the metal holder, and the metal tube with a diameter of 0.6 mm was fixed vertically. The metal tube's mouth on the beaker was rounded to create a 1 mm space between the liquid's surface and the nozzle. This is how Ag-Cr nanocomposites were made using the plasma process. Gradually increasing the voltage applied to the system, a plasma formed between the liquid's surface and the tube. The reduction of ions to basic silver and chromium shell was shown by the solution's gradual transformation to walnut hue. Then, the thin films were generated according to the setup shown in Fig. 1 of the homemade pyrolysis system to create a thin layer of silver nanoparticles with a shell and core that varied in the Ag@Cr ratio. The 2.5 x 2.5 cm glass substrates were cleaned using distilled water for 10 minutes, followed by acetone and ethanol for 20 minutes each in a Virionic digital cleaning machine. They were then dried for 10 minutes at 80°C. After the glass substrate was heated to 250 °C on a hot plate, the spray cell was filled with 35 mL of the nanoparticle silver and chrome solution. The nozzle used for spraying was 0.1 mm in diameter and was positioned on the glass substrate in a vertical orientation. For thin films, the spray time was 5 seconds and the pressure was 3.5 bar per layer; these parameters were then repeated for the other thin films.

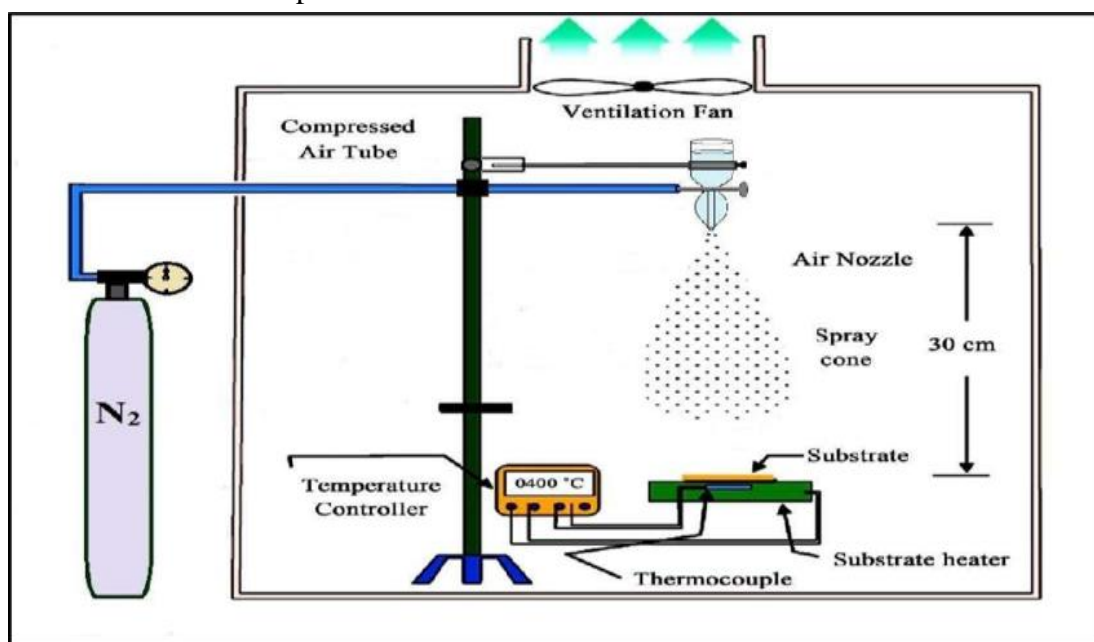


Figure 1: Homemade Spray Pyrolysis System for Nanoparticles Thin Films Preparation.

Sensor testing procedure: the test chamber was opened and the sensor was mounted on the heater. The pin feed and the sensor were electrically connected with conductive aluminum sheet; the test chamber was then closed. A bias voltage of six volts was set between the two sides of the linked electrodes; the test chamber was vacuumed to about 1 mbar with a rotary pump, and a temperature controller was used to set the sensor to the required working temperature. Fig. 2 shows a schematic diagram of the electrical circuit for gas sensing measurements. The flow rate of air and tested gas was adjusted using the needle valves, and a volumetric concentration of 5% test gas was added to air. A UNI-UT81B digital multimeter with a PC interface was used to measure current fluctuations.

The digital millimeter first measured the biasing current of air flow, then the testing gas (NO₂) was turned on, and after a few seconds, the current has little variation, the test gas was turned off to measure the recovery time.

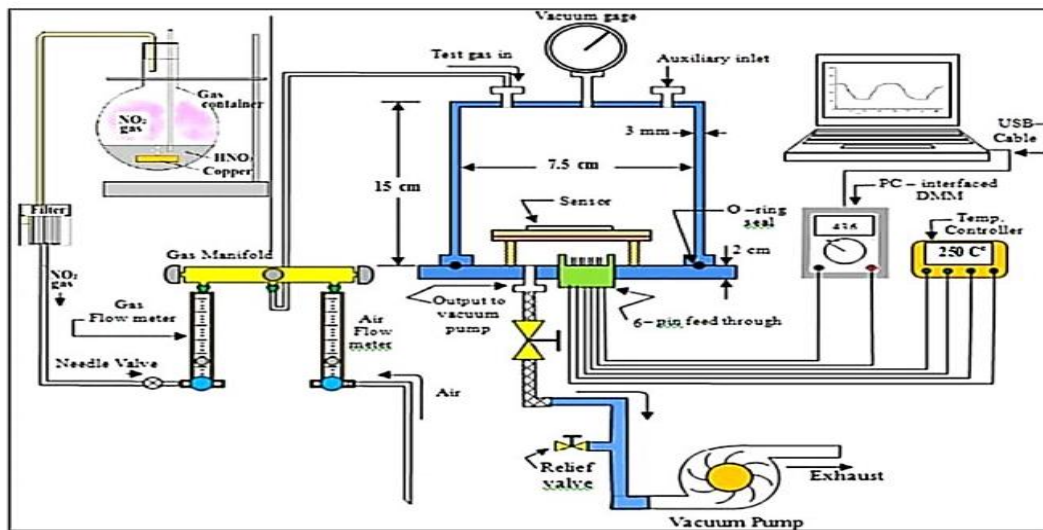


Figure 2: Diagram of Gas sensor set up [16].

3. Results and Discussion

The absorption behavior of the pure Ag NPs (10 mL) and Ag@Cr core-shell NPs of (2:8, 3:7, and 4:6) ratios were investigated by UV-visible spectroscopy. Fig. 3 displays the normalized absorption spectra of Ag and Ag@Cr nanocomposites obtained at room temperature within the 300–800 nm wavelength range. The absorption edge wavelengths for pure Ag was 424nm. This indicates the formation of Ag NPs due to the surface plasmon resonance (SPR) of Ag nanoparticles. The absorption edge wavelengths of Ag@Cr core-shell of different Ag:Cr ratios were 408, 413, and 410 nm. The absorption peaks increased with decreasing the wavelength [17-19].

Fig. 4 shows the XRD patterns of the as-synthesized Ag and Ag@Cr. According to JCPDS No. 04-0783, two peaks at $2\theta=38.15^\circ$ and 44.26° corresponding to the cubic Ag lattice planes (111) and (200), respectively, were noted, with a lattice constant of $a=4.086 \text{ \AA}$ [20-22]. Additionally, every additional reflection peak is precisely aligned with the cubic phase of Cr ($a= 5.24150 \text{ \AA}$), thereby validating the standard card (JCPDS No. 00-006-0694). The strongest peak among these was at $2\theta=58.34^\circ$ and 64.58 , which agrees well with the Cr crystalline planes (113) and (110). The crystallite size of all deposited films was calculated by the well-known Debye-Scherrer Eq. (2) [23, 24]

$$D = \frac{0.9 \lambda}{\beta \cos \theta} \quad (2)$$

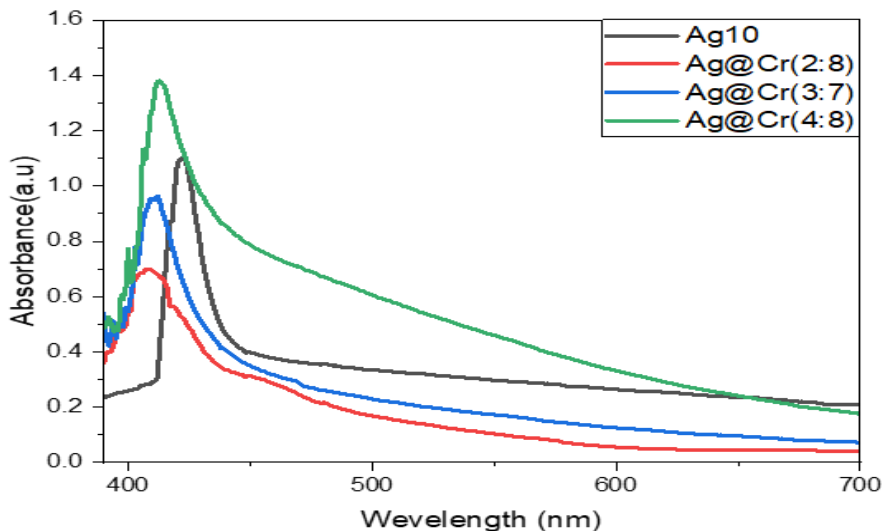


Figure 3: UV-visible spectra of Ag and Ag@Cr core-shell NPs.

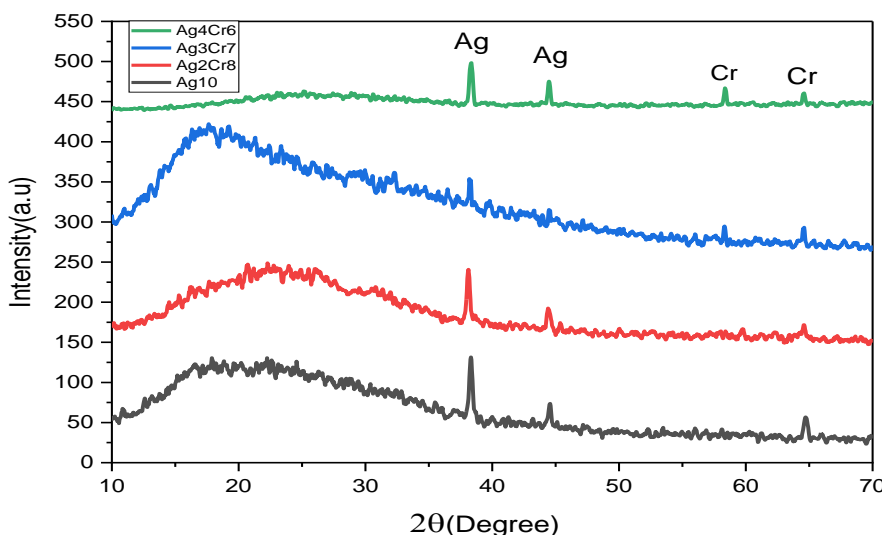


Figure 4: XRD of sputtered Ag@Cr thin films.

Transmission Electron Microscopy (TEM) revealed that the silver nanoparticles were of rounded-shape phases and core-shell (Ag/Cr) structures, as shown in Fig. 5. The particle size of the pure Ag particles was with a diameter of 34 nm [25]. Particle sizes of (Ag/Cr) core-shell samples were measured ranging between 40 nm to 70 nm. The core and shell can be seen in the TEM images; the silver appears in black, surrounded by the chrome appearing in white.

The sensitivity of the prepared films against NO₂ gas was examined at three distinct operating temperatures (150, 200, and 250 °C). Figs. 6, 7, 8, 9 and 10 (a, b and c) illustrate how the resistance of pure Ag and Ag@Cr films varied over time on exposure to NO₂ gas; the green and red arrows denoting gas-on and gas-off, respectively. The resistance of metal oxide semiconductor thin films increases with time after gas-off and decreases with time after gas-on, as seen in the figures. The sensitivity (S) was calculated using the following Eq (3)

$$S\% = (R_{on}(\Omega) - R_{off}(\Omega)) / R_{on}(\Omega) \times 100\% \tag{3}$$

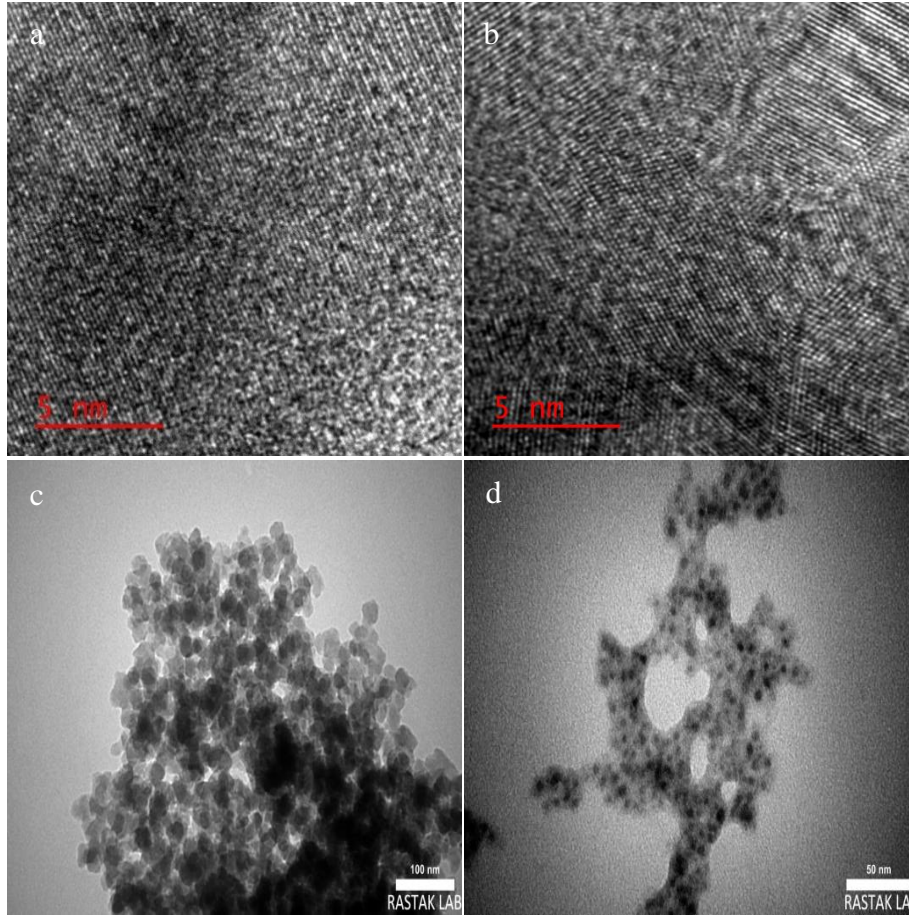


Figure 5: TEM Images of (a) Pure Ag, (b) Ag@Cr(2:8), (c) Ag@Cr(3:7), (d) Ag@Cr(4:6).

where R_{on} and R_{off} are the electrical resistance of the films in the existence of gas (gas-on) and in the air (gas-off), respectively [26, 27]. These figures explain why the resistance decreases with time after gas-on and increases with time after gas-off. The target gas interacts with the metal film's surface (usually through surface adsorbed oxygen ions), changing the material's concentration of charge carriers. The material's conductivity, also known as resistivity, is influenced by this shift in the concentration of charge carriers. An increase in conductivity and a decrease in resistivity are observed in P-type semiconductors, where the majority of charge carriers are holes. The reason for this is that when an oxidizing gas, such as NO_2 , is introduced, the oxygen ion extracts electrons from metal oxide, causing a decrease in resistance for all the samples under consideration. NO_2 is one type of oxidizing gas that reacts with the oxygen ion and keeps the electrons at the surface, increasing the concentration of holes inside. This indicates that after being exposed to NO_2 , the conductance of p-type metal oxide semiconductor would rise [28]. The interaction of a gas sensor with the molecules of the target gas determines the gas sensor's performance towards a given gas. Table 1 lists the sensitivity, response time, and recovery time for pure Ag, Ag@Cr films. Fig. 6 shows the sensitivity of the samples. It was noted that the sensitivity (Ag/Cr) core-shell films was lower than that of pure silver. The best sensitivity occurs at 150 K for all ratios, and the best sensitivity was for the core-shell (Ag/Cr) of 3:7 ratio. The best results for (Ag/Cr) of 3:7 ratio showed that the sensitivity at 150 K of operating temperature is 26.32% higher than other, with response time (24.3 sec), recovery time (45.9sec). This is owing to its porous nature, which increases the number of active sites and surface area for gas diffusion ratios and shows an improved gas response due to the high catalytic activity of the presence of spherical

silver nanoparticles. The sensitivity of pure silver at 150 K was 32.42%, with recovery time (46.8 sec), response time (20.7sec).

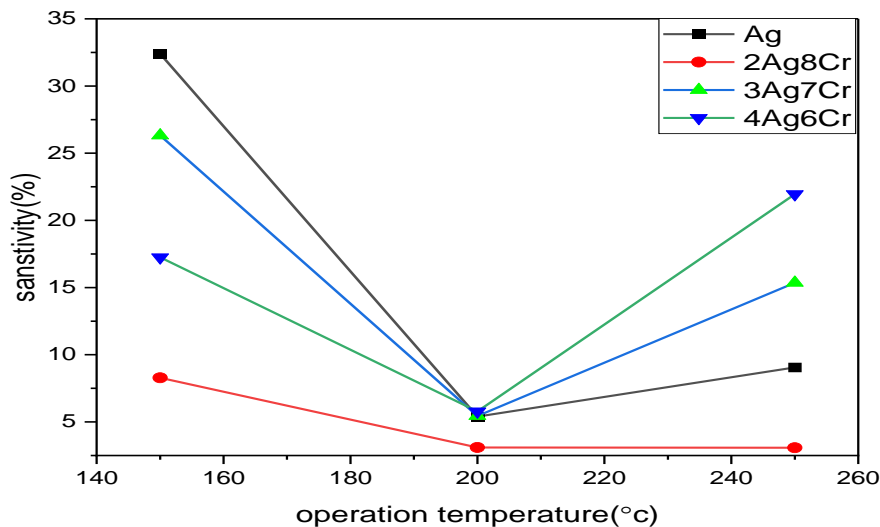


Figure 6: NO₂ gas sensitivity at different operating temperatures for the (Ag and Ag@Cr).

Table 1: Sensitivity, response and recovery time for (Ag, Ag@Cr) films at different operating temperatures for the detection of NO₂ gas.

Samples	Operating temp (°C)	S%	Response time (s)	Recover time (s)
Ag10	150	32.4	20.7	46.8
	200	5.40	19.8	46.8
	250	9.06	21.6	48.6
Ag2Cr8	150	8.28	20.7	50.4
	200	3.10	27	45
	250	3.08	29.7	42.3
Ag3Cr7	150	26.32	24.3	45.9
	200	5.44	29.7	38.7
	250	15.36	34.2	35.1
Ag4Cr6	150	17.25	14.4	57.6
	200	5.78	19.8	52.2
	250	21.95	21.6	48.6

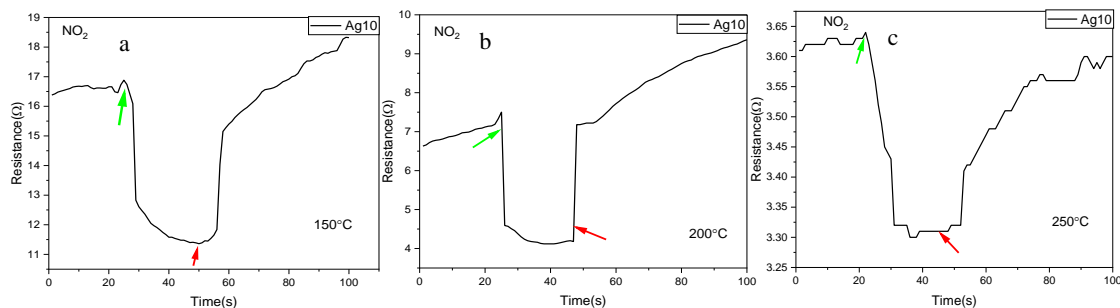


Figure 7: Changes in Ag thin film resistance to NO₂ gas at different operating temperatures of (a) 150, b) 200 and c) 250°C).

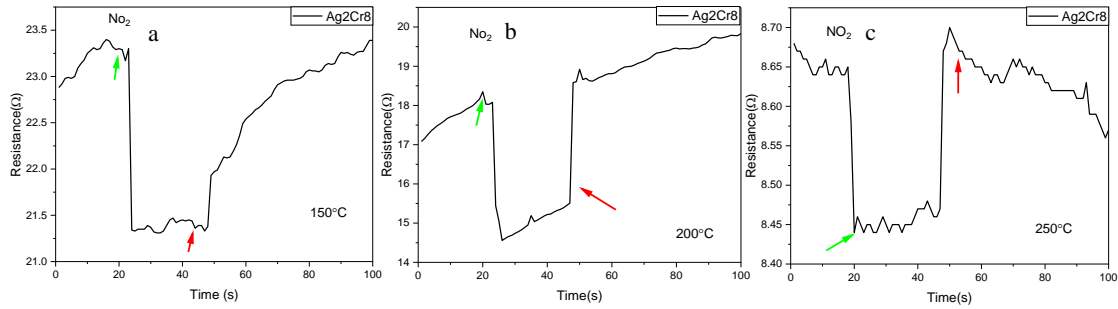


Figure 8: Changes in Ag@Cr(2:8) film resistance to NO₂ gas at different operating temperatures of (a) 150, b) 200 and c) 250°C).

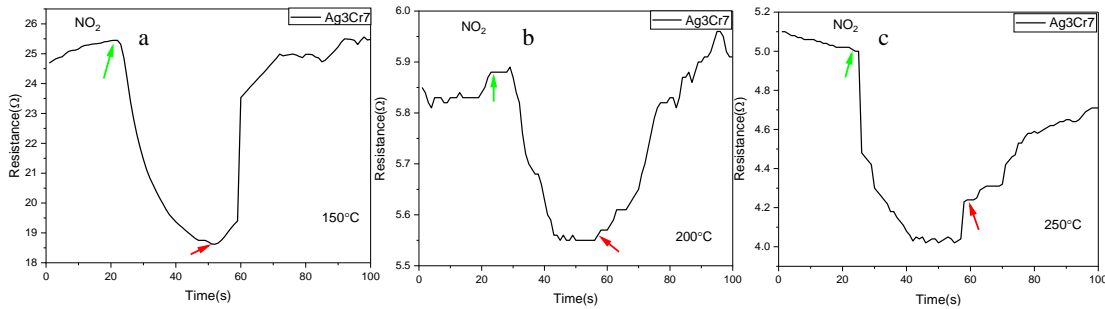


Figure 9: Changes in Ag@Cr(3:7) film resistance to NO₂ gas at different operating temperatures of (a) 150, b) 200 and c) 250°C).

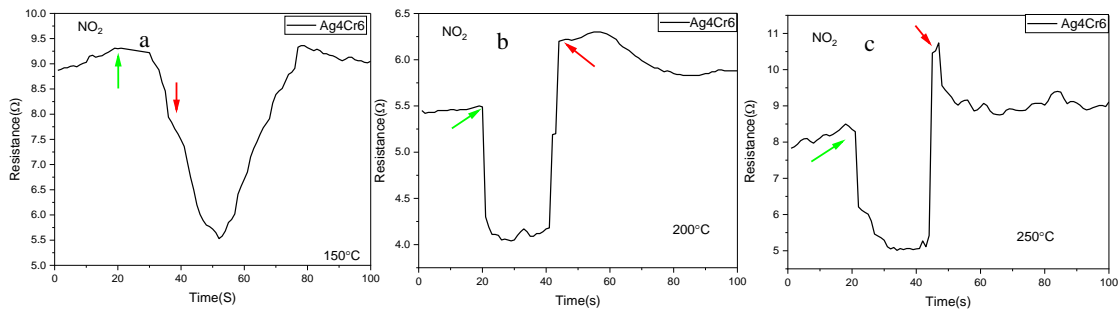


Figure 10: Changes in Ag@Cr(4:6) film resistance to NO₂ gas at different operating temperatures of (a) 150, b) 200 and c) 250°C).

Hall measurements revealed that the Ag@Cr deposited as a thin coating on the glass substrate was p-type semiconductor. The p-type films' Hall parameters included electrical conductivity (σ), Hall coefficient (RH), carrier concentration (nH), and mobility (μ H) are shown in Table 2.

Table 2: The Hall effect parameters for Ag@Cr.

Ag@Cr	σ ($\Omega \cdot \text{cm}^{-1}$)	RH	n (cm^{-3})	type	μ H ($\text{cm}^2/\text{v} \cdot \text{sec}$)
10:0	2.304E-05	1.946 E+06	3.208 E+7	P	44.83
2:8	2.049E-05	6.05 E+03	1.031 E+10	P	13.90
3:7	2 E-05	1.13 E+03	5.545 E+15	P	1.95E+3
4:6	2 E-05	7.06 E+02	8.840 E+15	p	2.07E+3

4. Conclusions

A dependable and adaptable method for creating Ag@Cr thin film gas sensors was the Spray Pyrolysis System. Silver to chromium had a significant impact on the prepared films' properties. Ag@Cr films were of tetragonal polycrystalline structure. At

temperatures (<150°C), the Ag@Cr thin film gas sensors performed better. Ag@Cr films produced in this work had a maximum gas sensitivity of about 26% at 150°C operating temperature. Using NO₂ gas resulted in shorter reaction and recovery times as the operating temperature rose.

Conflict of interest

The authors declare that they have no conflict of interest.

References

1. S. Genc, Z. Zadeoglulari, S. H. Fuss, and K. Genc, *J. Toxicol.* **2012**, 782462 (2012). DOI: 10.1155/2012/782462.
2. J. Brunet, V. P. Garcia, A. Pauly, C. Varenne, and B. Lauron, *Sens. Actuat. B Chem.* **134**, 632 (2008). DOI: 10.1016/j.snb.2008.06.010.
3. K. Victorin, *Mutat. Res./Rev. Gen. Toxicol.* **317**, 43 (1994). DOI: 10.1016/0165-1110(94)90011-6.
4. J. A. Bernstein, N. Alexis, C. Barnes, I. L. Bernstein, A. Nel, D. Peden, D. Diaz-Sanchez, S. M. Tarlo, P. B. Williams, and J. A. Bernstein, *J. Allerg. Clin. Immun.* **114**, 1116 (2004). DOI: 10.1016/j.jaci.2004.08.030.
5. G. Bhanjana, G. R. Chaudhary, N. Dilbaghi, M. Chauhan, K.-H. Kim, and S. Kumar, *Electrochim. Acta* **293**, 283 (2019). DOI: 10.1016/j.electacta.2018.10.042.
6. B. J. Murray, Q. Li, J. T. Newberg, J. C. Hemminger, and R. M. Penner, *Chem. Mat.* **17**, 6611 (2005). DOI: 10.1021/cm051647r.
7. S. H. Lee and B.-H. Jun, *Int. J. Mol. Sci.* **20**, 865 (2019). DOI: 10.3390/ijms20040865.
8. A. Loiseau, V. Asila, G. Boitel-Aullen, M. Lam, M. Salmain, and S. Boujday, *Biosensors* **9**, 78 (2019). DOI: 10.3390/bios9020078.
9. H. K. Mohaisen, J. Haji, A. M. Oda, H. A. Jabr, and M. A. Maithem, *J. Adv. Res. Dyn. Cont. Syst.* **12**, 228 (2020). DOI: 10.5373/JARDCS/V12I4/20201437.
10. M. Costa and C. B. Klein, *Crit. Rev. Toxicol.* **36**, 155 (2006). DOI: 10.1080/10408440500534032.
11. H. Jing, N. Large, Q. Zhang, and H. Wang, *J. Phys. Chem. C* **118**, 19948 (2014). DOI: 10.1021/jp5064116.
12. J. Xiong, Z. Li, J. Chen, S. Zhang, L. Wang, and S. Dou, *ACS Appl. Mat. Interf.* **6**, 15716 (2014). DOI: 10.1021/am502516s.
13. N. K. Abdalameer, S. N. Mazhir, and K. A. Aadim, *Ener. Rep.* **6**, 447 (2020). DOI: 10.1016/j.egy.2020.09.023.
14. B. Ding, M. Wang, J. Yu, and G. Sun *Gas Sensors Based on Electrospun Nanofibers*. *Sensors*, 2009. **9**, 1609 DOI: |.
15. S. Chopra, K. Mcguire, N. Gothard, A. M. Rao, and A. Pham, *Appl. Phys. Lett.* **83**, 2280 (2003). DOI: 10.1063/1.1610251.
16. A. J. R. Muhammed, M.Sc Thesis, University of Baghdad, 2021.
17. P. Rai, S. M. Majhi, Y.-T. Yu, and J.-H. Lee, *RSC Adv.* **5**, 17653 (2015). DOI: 10.1039/C4RA13971B.
18. R. A. Mohammed, G. M. Saleh, and F. A. Mutlak, *Iraqi J. Nat. Sci. Nanotech.* **3**, 44 (2022). DOI: 10.47758/ijn.vi3.53.
19. C. Chairanit, R. Patramanon, N. Phukkaphan, and T. Kerdcharoen, 16th International Conference on Electrical Engineering/Electronics, Computer, Telecommunications and Information Technology (ECTI CON) (Pattaya, Thailand 2019). p. 226.
20. X. Liu, X. Sun, X. Duan, C. Zhang, K. Zhao, and X. Xu, *Sens. Actuat. B Chem.* **305**, 127450 (2020). DOI: 10.1016/j.snb.2019.127450.
21. M. S. Mohammed, B. H. Adil, A. S. Obaid, and A. M. Al-Shammari, *Mat. Sci. For.* **1050**, 51 (2022). DOI: 10.4028/www.scientific.net/MSF.1050.51.
22. A. S. Mulekar, A. Themdeo, A. Kalambe, and S. Pande, *AIP Conf. Proc.* **2104**, 030019 (2019). DOI: 10.1063/1.5100446.
23. T. Çayır Taşdemirci, *Opt. Quant. Elect.* **51**, 245 (2019). DOI: 10.1007/s11082-019-1963-0.
24. J. N. Silva, J. Saade, P. M. A. Farias, and E. H. L. Falcão, *Adv. Nanopar.* **2**, 6 (2013). DOI: 10.4236/anp.2013.23030.
25. K. R. Devi, G. Selvan, M. Karunakaran, K. Kasirajan, M. Shkir, and S. Alfaify, *Superlatt. Microstruct.* **143**, 106547 (2020). DOI: 10.1016/j.spmi.2020.106547.
26. H. J. Akber, I. M. Ibrahim, and K. H. Razeg, *J. Phys.: Conf. Ser.* **1664**, 012017 (2020). DOI: 10.1088/1742-6596/1664/1/012017.
27. M. I. Hasan, N. A. Bakr, and I. M. Ibrahim, *J. Electron. Mater.* **50**, 2940 (2021). DOI: 10.1007/s11664-021-08839-2.

28. S. R. Gawali, V. L. Patil, V. G. Deonikar, S. S. Patil, D. R. Patil, P. S. Patil, and J. Pant, J. Phys. Chem. Sol. **114**, 28 (2018). DOI: 10.1016/j.jpics.2017.11.005.

تصنيع المركبات النانوية ذات القشرة الأساسية $Ag@Cr$ تطبيق الاستشعار غاز ثاني أكسيد النيتروجين

زهراء علي مقبل¹ وأشواق طارق دحام¹
¹قسم الفيزياء، كلية العلوم للبنات، جامعة بغداد، بغداد، العراق

الخلاصة

تم إنشاء أغشية رقيقة من $Ag@Cr$ و Ag في هذا العمل باستخدام طريقة الترسيب بالرش الكيميائي ونفث البلازما لتصنيع الجسيمات النانوية $Ag@Cr$ 4:6، $Ag@Cr$ 2:8، $Ag@Cr$ 3:7، و 10 مل للحصول على أفضل خصائص الكشف عن الغاز. ويتوفر أيضًا تحليل لخصائص XRD للأغشية الرقيقة $Ag@Cr$ و Ag . علاوة على ذلك، فإن أطراف امتصاص الأشعة فوق البنفسجية للأغشية الرقيقة تمتد من 400 إلى 700. وقد تم عرض الطبيعة متعددة البلورات للأفلام من خلال نمط XRD على الشاشة. تم اختبار الأغشية الرقيقة للمركبات النانوية $Ag@Cr$ باستخدام الغاز المؤكسد NO_2 لتحديد حساسيتها وزمن الاستجابة وزمن الاسترداد. أظهرت النتائج أن أفضل نسبة كانت 3:7 مع حساسية 26% عند 150 درجة مئوية. كانت حساسية الفضة النقية عند 150 درجة مئوية 32% ونستنتج أن الكروم لديه حساسية منخفضة. وأظهرت نتائج تأثير هول أن المادة من نوع p في جميع النسب.

الكلمات المفتاحية: ثاني أكسيد النيتروجين، مستشعر الغاز، النانو مركبات، $Ag@Cr$ ، واللب والقشرة.